


Noncryogenic Quantum Repeaters with hot Hybrid Alkali-Noble Gases

Jia-Wei Ji^{1,*}, Faezeh Kimiaee Asadi¹, Khabat Heshami^{2,3} and Christoph Simon^{1,†}

¹*Institute for Quantum Science and Technology, and Department of Physics & Astronomy, University of Calgary, 2500 University Drive NW, Calgary, Alberta T2N 1N4, Canada*

²*National Research Council of Canada, 100 Sussex Drive, Ottawa, Ontario K1A 0R6, Canada*

³*Department of Physics, University of Ottawa, Advanced Research Complex, 25 Templeton Street, Ottawa, Ontario K1N 6N5, Canada*

 (Received 17 October 2022; revised 17 January 2023; accepted 1 May 2023; published 19 May 2023)

We propose a quantum repeater architecture that can operate without cryogenics. Each node in our architecture builds on a cell of hot alkali atoms and noble-gas spins that offer an hours-long storage time. Such a cell of hybrid gases is placed in a ring cavity, which allows us to suppress the detrimental four-wave-mixing noise in the system. We investigate the protocol based on a single-photon source made of an ensemble of the same hot alkali atoms. A single photon emitted from the source is either stored in the memory or transmitted to the central station to be detected. We quantify the fidelity and success probability of generating entanglement between two remote ensembles of noble-gas spins by taking into account finite memory efficiency, channel loss, and dark counts in detectors. We describe how the entanglement can be extended to long distances via entanglement swapping operations by retrieving the stored signal. Moreover, we quantify the performance of this proposed repeater architecture in terms of repeater rates and overall entanglement fidelities and compare it to another recently proposed noncryogenic quantum repeater architecture based on nitrogen-vacancy (N-V) centers and optomechanical spin-photon interfaces. As the system requires a relatively simple setup, it is easier to perform multiplexing, which enables achieving rates comparable to the rates of repeaters with N-V centers and optomechanics, while the overall entanglement fidelities of the present scheme are higher than the fidelities of the previous scheme. Our work shows that a scalable long-distance quantum network made of hot hybrid atomic gases is within reach of current technological capabilities.

DOI: [10.1103/PhysRevApplied.19.054063](https://doi.org/10.1103/PhysRevApplied.19.054063)

I. INTRODUCTION

The realization of global quantum networks would bring many fascinating applications to the world, which include secure communication [1], blind quantum computing [2], private database queries [3], and eventually, a quantum internet that connects quantum computers and other quantum information processing devices [4–6]. In such a quantum network, photons are used as information carriers for establishing long-distance connections, but they are adversely affected by transmission loss, which significantly limits the distance of connecting remote locations. Unlike its classical counterparts, photon loss cannot be compensated by amplification as unknown quantum states cannot be perfectly cloned according to the no-cloning theorem [7]. Therefore, quantum repeaters have been proposed to solve this issue but this requires stationary quantum memories for storing and processing the quantum information

[5,8,9]. Currently, a vast majority of approaches to quantum networks need either vacuum equipment and optical trapping or cryogenic cooling [8,10–17], which makes scaling up such architectures very difficult. However, there have been some efforts in proposing quantum networks that operate at room temperature based on solid-state systems [18,19], but they require complex setups and have high demands in designing the hardware for realizing the spin-photon interface. On the other hand, hot alkali vapors have been actively investigated as quantum memories for the application of quantum networks [20–24], and as they require relatively simple setups, it is easier to scale, which even offers a great potential for being deployed in space [25].

In spite of the appealing features of hot alkali vapor, there are a few challenges in the system. The main roadblock towards using this system for quantum networks is four-wave-mixing (FWM) noise as it is quite significant and ubiquitous in Λ -type hot atomic ensembles, posing serious challenges to the single-photon level applications [26,27]. Proposed solutions to this issue include

*quantum.jiawei.ji@gmail.com

†christoph.simon@gmail.com

blocking FWM channels by polarization selection rules [28], Raman absorption-enabled suppression in a mixed hot vapor [29], cavity engineering [30], and by means of coherent destructive interference of FWM [31]. The advantage of using a cavity to suppress FWM noise compared with other solutions is that it offers enhanced light storage and retrieval efficiencies while only introducing a cavity. It has been experimentally verified, reporting a noise floor of around 1.5×10^{-2} photons per pulse in a Raman-type hot vapor memory [32]. Another significant challenge in the Λ -type hot atomic ensembles is short storage time in the collective spin state, which is mainly affected by the atomic collisions between the hot vapor and the buffer gas and the collisions in the hot vapor itself. Because of this detrimental effect, the storage time in hot ensembles is limited to a microsecond [33], thus restricting its application in quantum networks. However, there has been some work towards reducing this detrimental effect either by the motional averaging method [20,24] or by using a decoherence-free subspace of spin states [34] with the spin-coherence time extended to a second, but even a second-long coherence time may not be sufficient for long-distance quantum networks [8]. It is worth noting that a minute-long spin relaxation time in hot alkali atoms has already been achieved [35], but no light storage was demonstrated in this experiment.

Rare isotopes of a noble gas have nonzero nuclear spins, which are isolated from the environment by electronic shells. Thus, they maintain hours-long coherence time even at room temperature [36]. They can be accessed either via the collisions with metastable helium atoms or via the collisions with alkali atoms [36]. A quantum interface between noble-gas spins and alkali atoms has been proposed based on weak spin-exchange collisions [37]. Using this interface, the storage time can be significantly enhanced, which has been experimentally demonstrated with the coherence time of a minute [38] and an hour [39].

In this work we propose a quantum repeater architecture without cryogenics, which is based on hot alkali vapor and noble-gas nuclear spins. In our proposal we adopt the cavity engineering method to suppress FWM noise when the input gets stored as a collective spin excitation in hot vapor via the off-resonant Raman protocol [30], and then it is mapped to noble-gas spins via weak spin-exchange collisions [37,40]. We consider the single-photon-based protocol [8] where single-photon sources and quantum memories are used for entanglement generation and swapping. We propose to use the same hot alkali atomic ensembles for single-photon sources. We quantify and analyze the entanglement generation efficiency and fidelity between two remote ensembles of noble-gas spins. Then, we show how entanglement swapping can be done to extend the entanglement to longer distances. Finally, we compute the repeater rates and overall fidelities and

compare them to quantum repeaters with N-V centers and optomechanics.

This paper is organized as follows. In Sec. II we introduce the hybrid system of hot vapor and noble-gas spins in a ring cavity. The single-photon protocol is presented in Sec. III. Section IV discusses the repeater rates and fidelities. Section V gives more details on system implementation. We conclude and provide an outlook in Sec. VI.

II. HYBRID ATOMIC GAS SYSTEM

As shown in Fig. 1(a), the hybrid atomic gas system is composed of a ring cavity and a cell of two hot atomic gases: alkali atoms and noble-gas atoms. This cell placed inside the cavity is driven by the control field (red) and the Stokes field (green). The ring cavity consists of two fully reflective mirrors and a mirror that serves as an input-output coupler with amplitude reflectivity r . The coherent interaction between the noble-gas spins and alkali atoms is achieved by spin-exchange collisions [37]. As shown in Fig. 2, an ensemble of alkali atoms is modeled as a Λ -type system with a collective ground state $|g\rangle$, a collective spin state $|s\rangle$, and an excited state $|e\rangle$. Each noble-gas atom is modeled as a spin-1/2 system with up and down states $|\uparrow\rangle$, $|\downarrow\rangle$. Here, we denote the collective noble-gas spin state as $|k\rangle$. The input signal (Stokes field) S couples the $|g\rangle$ - $|e\rangle$ transition with the strength proportional to the density of alkali atoms n_a , and the control field couples to the $|e\rangle$ - $|s\rangle$ transition with the Rabi frequency $\Omega(t)$. Both fields are detuned from $|e\rangle$ by Δ_s . The control field can also couple the $|g\rangle$ - $|e\rangle$ transition with the detuning of Δ_a , which generates the anti-Stokes field A (FWM noise) because here all alkali atoms are prepared in one of the ground states that has higher energy [30]. Because of the effect of spatial diffusion, there could be many spatial modes for the alkali and noble gases. However, in the light-dominated regime where the power broadening in the alkali atoms due to the control beam dominates over diffusion in the alkali atoms, the collective spin mode of the alkali gas and the collective spin mode of the noble gas can be well approximated as single uniform modes by engineering the spatial profile of the control field [40]. This condition is satisfied in this work, which is discussed in detail in Sec. V.

We need to polarize both the alkali and noble gases along the vertical axis. The former can be done using standard optical pumping, and the latter can be done using spin-exchange optical pumping (SEOP). The SEOP takes around 10 h to complete, but this preparation can last up to 100 h. The collective alkali spin state $|s\rangle$ can be coupled to the collective noble-gas spin state $|k\rangle$ via a weak spin-exchange collision with the strength J . The coupling strength J is given by $J = \zeta \sqrt{(2I + 1)p_a p_b n_a n_b} / 4$, where ζ is the local average interaction strength of an alkali-noble

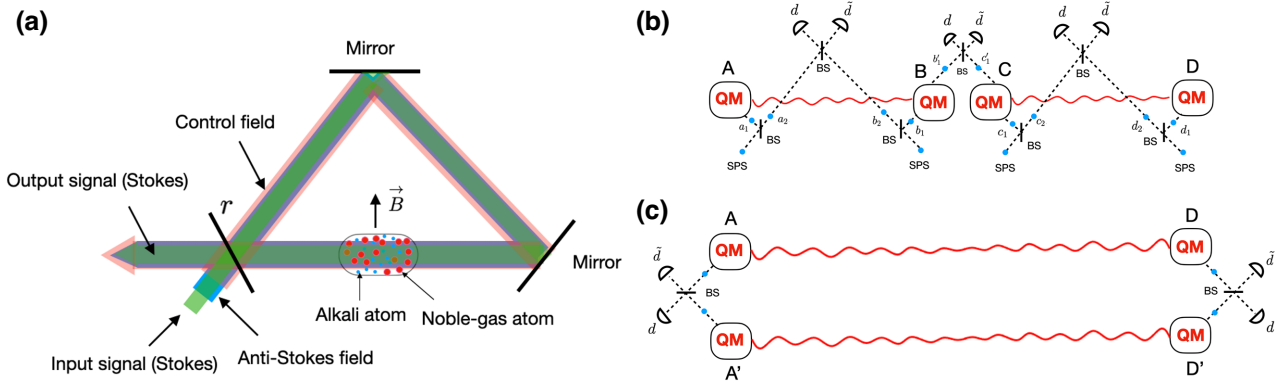


FIG. 1. (a) Schematic of the setup of hybrid quantum memories. A cell that contains alkali atoms (red dots) and noble-gas atoms (blue dots) is placed inside a ring cavity where the green signal and red control field interact with alkali atoms directly. The FWM noise is the generated blue anti-Stokes field during the storage and retrieval processes, which can be largely suppressed via tuning the cavity. The interface between alkali atoms and noble-gas spins is based on spin-exchange collisions. (b) Schematic of a two-link repeater with single-photon sources [41] as an example. There are two elementary links with four nodes and each one has a single-photon source that is a hot alkali atomic ensemble, a beam splitter, and a hot alkali-noble gases hybrid system serving as a quantum memory. The single-photon source emits a photon that either transmits through the beam splitter or gets reflected to enter the quantum memory. Two steps are required to establish the entanglement between nodes A and D. The first step is to generate the entanglement between A and B, C and D. The second step is to perform the entanglement swapping between B and C to distribute the entanglement to A and D. (c) Schematic of post-selection. This is the same as in the Duan-Lukin-Cirac-Zoller (DLCZ) protocol [10]. The entanglement is established both in links A-D and A'-D', and the stored photons are retrieved to be detected, which allows us to rotate the measurement basis by adjusting the transmission coefficients and phases of the beam splitters [8].

atom pair in a single collision, and p_a and p_b are the polarization degrees of alkali and noble gases, and n_a and n_b are the densities of alkali and noble gases in the cell. Here I is the nuclear spin of an alkali atom. Thus, J is the effective interaction strength in multiple collisions with each collision averaging over all alkali-noble atom pairs in the ensembles [37]. The detuning between these two states is δ_k , which can be tuned by applying a magnetic field along the vertical axis. This detuning can be used to decouple these two species of atoms [37,39]. Here γ_e , γ_s , and γ_k are the decoherence rates for the collective excited state, spin state, and noble-gas spin state, respectively. Moreover, we have $\gamma_k \ll \gamma_s$ as noble-gas spins have an extremely low decoherence rate.

The Maxwell-Bloch equations of this hybrid system with the excited state $|e\rangle$ being adiabatically eliminated take the form [30,40]

$$\begin{aligned}
 (c\partial_z + \partial_t)S &= ic\sqrt{\frac{d\gamma_e}{L_c}} \frac{\Omega}{\Gamma_s} B - \kappa_s S, \\
 (c\partial_z + \partial_t)A &= ic\sqrt{\frac{d\gamma_e}{L_c}} \frac{\Omega}{\Gamma_a} B^\dagger - \kappa_a A, \\
 \partial_t B &= -i\sqrt{\frac{d\gamma_e}{L_c}} \frac{\Omega^*}{\Gamma_s} S + i\sqrt{\frac{d\gamma_e}{L_c}} \frac{\Omega}{\Gamma_a} A^\dagger \\
 &\quad - \left(\frac{1}{\Gamma_s} + \frac{1}{\Gamma_a^*} \right) |\Omega|^2 B - \gamma_s B - iJK,
 \end{aligned}$$

$$\partial_t K = -(\gamma_k + i\delta_k)K - iJB, \quad (1)$$

where S , A , B , and K are the annihilation operators for the signal field, anti-Stokes field, bosonic collective spin wave, and collective noble-gas spin wave (we use the same notation as in Ref. [37]). Here $\Gamma_{s,a} = \gamma_e - i\Delta_{s,a}$ is the complex detuning of the signal and anti-Stokes fields. The optical depth is $d \propto g^2 p_a N_a / \gamma_e$, where N_a is the total number of alkali atoms inside the cell and g is the average coupling strength between the Stokes (anti-Stokes) fields and the alkali atoms, which is given by $g = \sqrt{1/N_a \sum_{i=1}^{N_a} |g_i(r_i)|^2}$. This approximation is valid when the number of excitations is much smaller than N_a [42], which is the case here. The length of a roundtrip in the cavity is L_c and c is the speed of light. The coordinate z indicates the direction along the optical path inside the cavity. Moreover, the bosonic operators B and K take the form $B(z, t) = e^{i\omega_{gs}(t-z/c)} \sum_{j \in [z, z+\delta z]} |g\rangle_j \langle s| / (\delta z \sqrt{p_a n_a})$ and $K = e^{i\delta_k(t-z/c)} \sum_{i \in [z, z+\delta z]} |\downarrow\rangle_i \langle \uparrow| / (\delta z \sqrt{p_b n_b})$. As mentioned before, the spin-exchange coupling rate J is proportional to the densities of the two atomic gases n_a and n_b , i.e., $J \propto \sqrt{n_a n_b}$ [37]. Thus, by increasing the pressure, one can increase this interaction strength. Here $\kappa_s = cd\gamma_e / (L_c \Gamma_s)$ and $\kappa_a = cd\gamma_e / (L_c \Gamma_a^+)$ stand for the decay rates of the Stokes field and anti-Stokes field in the ring cavity, where $\Gamma_a^+ = \gamma_e - i(\Delta_a + \delta_s)$ with δ_s being the splitting between the states $|g\rangle$ and $|s\rangle$. Strictly speaking, Eq. (1) should also have the Langevin noise operators. However, for both the signal

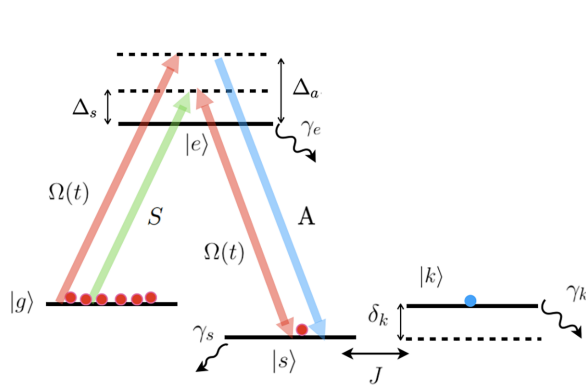


FIG. 2. The level diagram of a hybrid system with hot vapor and noble gases. The $|g\rangle$ - $|e\rangle$ transition is coupled by the input signal (Stokes field) with the strength proportional to $\sqrt{n_a}$, where n_a is the number density of alkali atoms in the cell. The control field is coupled to the $|e\rangle$ - $|s\rangle$ transition with a time-dependent Rabi frequency $\Omega(t)$. Both fields are detuned from $|e\rangle$ by Δ_s , and the control field can also couple the $|g\rangle$ - $|e\rangle$ transition with the detuning Δ_a , which generates the anti-Stokes field A. The collective spin state for noble-gas atoms is denoted by $|k\rangle$. The $|s\rangle$ - $|k\rangle$ transition is coupled to each other via the spin-exchange collision with a constant strength J when these two states are in resonance with other, i.e., $\delta_k = 0$. The collective excited state, alkali spin state, and noble-gas spin state decohere at the rates of γ_e , γ_s , and γ_k , respectively. Typically, $\gamma_k \ll \gamma_s$ as noble-gas spins have extremely low decoherence rates.

and the anti-Stokes field, the noise is vacuum noise that is zero in normal ordering [43]. The first two equations in the above set of equations describe the dynamics of the signal and anti-Stokes field inside the cavity, and the third equation describes the dynamics of the density of the collective spin state of the alkali atoms, which couples not only to the signal and anti-Stokes field but also to the noble-gas spins. The last equation describes the dynamics of the density of the noble-gas spin state.

Now, we have the boundary condition where the intracavity fields S_0 and A_0 ($z = 0$) can be related to the input fields S_{in} , A_{in} and the fields at $z = L_c$: S_{L_c} and A_{L_c} by the input-output coupler. Thus, we obtain the following relations [30]:

$$\begin{aligned} S_0 &= r e^{i k_s L_c} S_{L_c} + t_r S_{\text{in}}, \\ A_0 &= r e^{i k_a L_c} A_{L_c} + t_r A_{\text{in}}. \end{aligned} \quad (2)$$

Here $t_r = \sqrt{1 - r^2}$ is the transmission coefficient of the coupler, and k_s and k_a are the wave vectors of the signal and the anti-Stokes fields, respectively. Moreover, S_{L_c} and A_{L_c} can be directly related to S_0 and A_0 by Taylor expansion. To the first-order approximation, we have

$$S_{L_c} \approx e^{-k_s \frac{L_c}{c}} \left(S_0 + i L_c \sqrt{\frac{d\gamma_e}{L_c} \frac{\Omega}{\Gamma_s}} B_0 - \frac{L_c}{c} \partial_t S_0 \right),$$

$$A_{L_c} \approx e^{-k_a \frac{L_c}{c}} \left(A_0 + i L_c \sqrt{\frac{d\gamma_e}{L_c} \frac{\Omega}{\Gamma_a}} B_0^\dagger - \frac{L_c}{c} \partial_t A_0 \right), \quad (3)$$

where B_0 is the collective alkali spin operator for $z = 0$. Combining these two sets of relations, one can obtain the following Maxwell-Bloch equations:

$$\begin{aligned} \partial_t s &= -\tilde{\kappa}_s s + i \sqrt{\frac{d\gamma_e}{\tau} \frac{\Omega}{\Gamma_s}} b + e^{-i\phi_s} \frac{t_r}{\mu_a \sqrt{\tau}} S_{\text{in}}, \\ \partial_t a &= -\tilde{\kappa}_a a + i \sqrt{\frac{d\gamma_e}{\tau} \frac{\Omega}{\Gamma_a}} a + e^{-i\phi_a} \frac{t_r}{\mu_a \sqrt{\tau}} A_{\text{in}}, \\ \partial_t b &= -\gamma_s b + i \sqrt{\frac{d\gamma_e}{\tau}} \left(-\frac{\Omega^*}{\Gamma_s} s + \frac{\Omega}{\Gamma_a} a \right) \\ &\quad - \left(\frac{1}{\Gamma_s} + \frac{1}{\Gamma_a^*} \right) |\Omega|^2 b - i J k, \\ \partial_t k &= -(\gamma_k + i\delta_k) k - i J b. \end{aligned} \quad (4)$$

Here $\tau = L_c/c$ is the cavity roundtrip time; $s = \sqrt{\tau} S_0$, $a = \sqrt{\tau} A_0$, $b = \sqrt{L_c} B_0$, and $k = \sqrt{L_c} K_0$ (K_0 is obtained by setting $z = 0$ in K) are the intracavity amplitudes for the signal, anti-Stokes field, collective alkali spin state, and collective noble-gas spin state, respectively; $\tilde{\kappa}_{s,a}$ is the resonant and antiresonant decay rates for the signal and anti-Stokes field. They are given by [30]

$$\frac{1}{\tilde{\kappa}_{s,a}} = \tau \frac{\mu_{s,a} e^{i\phi_{s,a}}}{1 - \mu_{s,a} e^{i\phi_{s,a}}}, \quad (5)$$

where $\phi_{s,a} = k_{s,a} L_c - \text{Im}\{\kappa_{s,a}\} \tau$ is the accumulated phases in the cavity roundtrip by the signal and anti-Stokes fields, and $\mu_{s,a} = r e^{-\text{Re}\{\kappa_{s,a}\} \tau}$ is the cavity roundtrip amplitude transmission for the fields.

Equation (4) can be solved in the bad-cavity regime where the signal (anti-Stokes) field evolved at a rate much slower than the corresponding decay rate, i.e., $|\tilde{\kappa}_{s,a}| \gg |\sqrt{d\gamma_e/\tau} \Omega / \Gamma_{s,a}|$ [43]. In this limit, we can set $\partial_t a \approx 0$ and $\partial_t s \approx 0$. Moreover, as we can decouple the alkali and noble gases by applying a large magnetic field, we can break the storage into two steps: first consider the storage in the alkali atoms in the presence of the anti-Stokes field and then consider the transfer from the alkali to the noble gas. This sequential storage is optimal when the signal pulse duration T satisfies $T \ll 1/\gamma_s$ [40], which is adopted in this work. We discuss how this sequential storage is achieved in detail and the optimal storage efficiency in Sec. III A. The main noise present in the system is FWM, and in order to achieve the maximum suppression of this noise, we need to tune the ring cavity to be in resonance with the signal and to be in antiresonance with the anti-Stokes field, which means $\phi_s = 0$ and $\phi_a = \pi$. This is crucial in the first step of storage and retrieval, which is discussed in more detail

in Sec. III B. Other sources of noise in hot vapor systems include collision-induced fluorescence noise, the Doppler broadening, and inhomogeneous broadening for the $|g\rangle$ - $|e\rangle$ transition. However, in this system we ignore these effects as it has been demonstrated that fluorescence noise is negligible for the off-resonant scheme with a short pulse input [44], and this is also true for the Doppler broadening and inhomogeneous broadening with the detuning Δ_s much larger than their bandwidth, which is discussed in Sec. V.

III. THE SINGLE-PHOTON REPEATER

Here, we focus on the single-photon-based protocol [41] for entanglement generation and entanglement swapping where each node consists of a beam splitter, a single-photon source, and a hybrid quantum system as depicted in Fig. 1(b), where we just show a two-link repeater as an example. As the noble-gas spins offer ultralong coherence time at room temperature, they will be used as the memory for storing the signal. There are two steps to establish the entanglement between two remote locations, and Fig. 1(a) shows how to achieve this between nodes A and D by cutting this distance into small pieces of equal length. In Fig. 1(b) it is cut into two equal pieces: A-B and C-D, but it can be more general to have more links. In this example, we need to first establish the entanglement between A and B, and C and D, which is called entanglement generation, and then we perform the entanglement swapping between two local memories B and C to distribute the entanglement to A and D, i.e., only entangling A and D. Moreover, as a single excitation in the noble-gas spins is shared between A and D, it is difficult to perform measurements in other bases than the basis $\{|k\rangle, |0\rangle\}$. In order to relax this, we can introduce another entangled link $A'D'$ where nodes A' and D' are in the same locations as A and D, respectively [41], which is depicted in Fig. 1(c). In this way, we can use two beam splitters and two detectors in each location to read out the stored photons, which allows measurements in an arbitrary basis by choosing the transmission coefficients and phases. This step is known as post-selection. In this section we show how entanglement generation, entanglement swapping, and post-selection can be achieved in our hybrid system, and we also quantify the established entanglement generation fidelity and efficiency in the elementary link.

A. Entanglement generation

Before we characterize how the entanglement generation can be done, we would like to first talk about how signal storage can be achieved and show what the optimal storage efficiency is. Our goal is to store the signal in the quantum memory as a collective excitation in the noble-gas spins, and this process can be divided into two steps: storing the signal in the collective spin excitation of

alkali atoms and transferring this excitation to the collective excitation in noble-gas spins. This sequential storage is optimal when the signal pulse duration T satisfies $T \ll 1/\gamma_s$ [40]. In order to execute the first step, we make the detuning δ_k between $|s\rangle$ and $|k\rangle$ large enough such that $\delta_k \gg J$, and when this condition is satisfied, the states $|s\rangle$ and $|k\rangle$ are decoupled from each other [37]. Then, this process is simply described by the first three equations in Eq. (4) with $J = 0$. Given that the maximum suppression of noise is achieved by tuning the ring cavity to be in resonance with the signal and to be in antiresonance with the anti-Stokes field ($\phi_s = 0$ and $\phi_a = \pi$), it has been shown that the optimal storage efficiency in the first step is $\eta_1 = 1 - \sqrt{d}\gamma_e/(\sqrt{2}\Delta_s)$ in the strong-coupling regime (see Sec. III B for more details) and the far-detuned regime ($\Delta_s \gg \gamma_e$) without mode mismatch in the cavity [30]. This efficiency could be achieved when using lossless optical components. The requirements for all the related parameters can be realized experimentally, which are discussed in Sec. V. It is worth noting that this optimal efficiency depends on the signal detuning Δ_s , as opposed to the previous result in [43] where the optimal efficiency was found to be detuning independent in the absence of FWM. The second step is to transfer the signal stored in the alkali atoms to the noble-gas spins. Thus, we need to turn off the control field $\Omega(t)$ and tune $|k\rangle$ on resonance with $|s\rangle$ to make them interact, which can be done using an external magnetic field [39]. The efficiency of this transfer is maximized when the transfer time is set to be $\pi/(2J)$ and it is in the strong coherent coupling regime, i.e., $J \gg \gamma_s \gg \gamma_k$ [40]. Then, we obtain the optimal transfer efficiency $\eta_2 = \exp(-(\pi(\gamma_s + \gamma_k))/2J)$, which gives us the following total storage efficiency:

$$\eta_s = \eta_1 \eta_2 = \left(1 - \frac{\sqrt{d}\gamma_e}{\sqrt{2}\Delta_s}\right) \exp\left(-\frac{\pi(\gamma_s + \gamma_k)}{2J}\right). \quad (6)$$

Now, we shall see how entanglement can be established in an elementary link. There are two links illustrated in Fig. 1(b), and here we focus on the first link for describing how the entanglement generation is achieved. In this link, for the left node, a single photon emitted from the source after a beam splitter can be described as $(\alpha a_1^\dagger + \beta a_2^\dagger)|0\rangle$, where α, β are reflection and transmission amplitudes of a beam splitter, and they satisfy the relation $|\alpha|^2 + |\beta|^2 = 1$. The same is true for the right node where the state of a single photon after a beam splitter is $(\alpha b_1^\dagger + \beta b_2^\dagger)|0\rangle$. Thus, the joint state is given by

$$[\alpha^2 a_1^\dagger b_1^\dagger + \alpha\beta(a_1^\dagger b_2^\dagger + a_2^\dagger b_1^\dagger) + \beta^2 a_2^\dagger b_2^\dagger]|0\rangle. \quad (7)$$

The first term in this state is the case where both single photons are reflected to be stored in quantum memories, ideally yielding no heralding in detectors. However, the

detector dark counts could potentially lead to spurious clicks, thus causing infidelity in the desired entangled state. This probability is given by $\epsilon_0(1 - \epsilon_0)\alpha^4$, where ϵ_0 is the probability of having no dark counts in detectors. Here, we take it into account, but later on, we see that its effect can be negligible if we choose the detector and detection window time properly. The second and third terms are the main contributions to single photon heralding where a_1^\dagger and b_1^\dagger are to be stored in quantum memories. We use noble-gas nuclear spins as quantum memories where the storage of a single photon is achieved in two steps as described above. As the finite storage efficiency, η_s , could create vacuum components, we take it into consideration in this work. The probability of having this contribution is given by $\epsilon_0\alpha^2\beta^2\eta_t\eta_c\eta_d\eta_s$, where η_t, η_d, η_c are the transmission, detection, and frequency conversion efficiencies. The last term could also lead to the single-photon detection event when one of the two photons gets lost in the transmission, thus creating vacuum components as well. As discussed in Sec. III B, although the hindsight from post-selection tells us that the vacuum components can be eliminated, which seems to have no effect on overall fidelity, it could still decrease the overall repeater rates. This probability is given by $\epsilon_0\beta^4\eta_t\eta_c\eta_d(1 - \eta_t\eta_c)$. Moreover, we assume that the probability that the single-photon source emits a photon is p_1 , which depends on the source we use.

Here, we choose to use the same hot alkali gas as a single-photon source, which can be charged with a single excitation via the FWM process used in the DLCZ protocol [10], and this atomic excitation can then be reverted to emit a single photon. A few experimental works have been reported for using hot rubidium atoms to generate bright and indistinguishable photons [45,46]. In this way, we do not need to perform frequency conversion to match with the alkali gas we use in the system, but the frequency conversion is needed for long-distance communication, i.e., for a_2 and b_2 . Using atomic ensembles to generate single photons could lead to multiphoton errors, thus degrading the repeater fidelities. This is discussed in detail in Sec. IV. We envision using the reverse-proton exchange periodically poled lithium niobate waveguide technique to convert a single photon emitted from the source to a telecom photon, which can operate at room temperature with a conversion efficiency of 23% for the 863 nm signal [47], but it is promising to apply it to signals of different wavelengths. Moreover, by choosing the proper waveguide mode filter and fiber type, one can greatly improve this conversion efficiency to 60% [47], and we use a higher value of 80% in Sec. IV for rate calculations. Also, we assume that the relative phase in two optical fibers remains stable. Practically, this requirement can be achieved by actively stabilizing the lengths of the fiber [8], or through the use of self-compensating Sagnac-type configurations [48].

After taking all these effects into account, the entanglement generation fidelity and efficiency of the state created by detecting a single photon in one of the detectors are given by

$$F_{\text{gen}} = \frac{\alpha^2\beta^2\eta_t\eta_c\eta_d\eta_s}{\beta^2\eta_t\eta_c\eta_d + (1 - \epsilon_0)\alpha^4 - \beta^4\eta_t^2\eta_c^2\eta_d}, \quad (8)$$

$$\eta_{\text{gen}} = 2p_1(\epsilon_0\beta^2\eta_t\eta_c\eta_d + \epsilon_0(1 - \epsilon_0)\alpha^4 - \epsilon_0\beta^4\eta_t^2\eta_c^2\eta_d), \quad (9)$$

where $\epsilon_0 = \exp(-\lambda T_d)$ with λ being the dark count rate and T_d the detection window time that is set to be the time duration of the signal, that is, $T_d = T$. η_t is the function of the length of an elementary link L_0 , which takes the following form: $\eta_t = \exp(-L_0/2L_{\text{att}})$ with $L_{\text{att}} = 22$ km being the attenuation length for telecom photons. The factor of 2 in the efficiency expression comes from the fact that the detectors are symmetric, and the heralding in either of them contributes to the efficiency. We envision using silicon single-photon avalanche diodes (Si SPADs) [49,50] and frequency conversion to detect telecom photons. Si SPADs combined with a monolithic integrated circuit of active quenching and active reset can enable detection efficiency as high as 75% with dark count rates below 100 Hz at 785 nm [49]. This type of detector can operate at non-cryogenic temperatures that only require a thermoelectric cooler. The parameters are taken to be $\alpha^2 = 0.84$, $\beta^2 = 0.16$, $\eta_d = 0.6$, $\eta_c = 0.8$, $T_d \sim 12.5$ ns (the signal bandwidth is around 80 MHz, which is compatible with the hot vapor bandwidth as discussed in Sec. V). In this regime, the term $(1 - \epsilon_0)\alpha^4$ is a few orders of magnitude smaller than $\beta^2\eta_t\eta_c\eta_d$ so Eq. (9) can be approximately written as $F_{\text{gen}} \approx \alpha^2\eta_s$, and $\eta_{\text{gen}} \approx 2p_1\beta^2\eta_t\eta_c\eta_d$. Moreover, we can now write the entangled state for each elementary link as

$$\alpha^2\eta_s |\psi_{ab}\rangle \langle\psi_{ab}| + [\alpha^2(1 - \eta_s) + \beta^2] |0\rangle \langle 0|, \quad (10)$$

where $|\psi_{ab}\rangle = 1/\sqrt{2}(|k_a\rangle |0_b\rangle + |0_a\rangle |k_b\rangle)$. The storage inefficiency $1 - \eta_s$ increases the vacuum component proportion and, therefore, it decreases the repeater rates. The required input pulse is short as it satisfies the condition $T \ll 1/\gamma_s$, which is also the requirement for the optimal signal storage in noble-gas spins using the sequential scheme [40]. Moreover, when we have two elementary links, there is some waiting time for both links to establish entanglement, and as noble-gas spins offer ultralong coherence time, the decoherence that happens during the waiting time is ignored.

B. Entanglement swapping

After we successfully establish the entanglement in two adjacent elementary links as shown in Fig. 1(b), we then

need to perform entanglement swapping to propagate the entanglement between A and D. This can be done by recalling the single photon stored in either quantum memories B or C that are in the same location, and the heralding at one of the beam splitters informs us of the success in the swapping process, leading to the entangled state shared between A and D. At this level, it is well known that the swapping probability takes the form [8]

$$P_1 = \frac{p_1 F_{\text{gen}} \eta}{2} (2 - p_1 F_{\text{gen}} \eta), \quad (11)$$

where $\eta = \eta_d \eta_r$ is the product of the detection efficiency and the retrieval efficiency. Here, the retrieval process happens in two phases as well. First, we map the excitation in noble-gas spins to the excitation in hot vapor via the spin-exchange interaction by turning on the magnetic field for the amount of time of $\pi/(2J)$ [37,40]. Second, we need to read out the signal from the collective spin state of the hot vapor. In this process, we need to turn on the control field $\Omega(t)$ and decouple the hot vapor from the noble gas by applying an external magnetic field to detune $|s\rangle$ from $|k\rangle$. The efficiency of retrieving the signal from hot vapor is the same as η_1 , and it only holds under the condition that the decoherence of $|s\rangle$ is negligible during this process, which is true as the decoherence happens on the time scale much slower than that of memory interactions [30,40]. Thus, the overall retrieval efficiency is $\eta_r = \eta_s$, which is given in Eq. (6).

Now, putting all together, we can further simplify Eq. (11) as $P_1 = p_1 \alpha^2 \eta_{\text{tot}} (1 - 1/(2)p_1 \alpha^2 \eta_{\text{tot}})$, where $\eta_{\text{tot}} = \eta_s \eta_r \eta_d$. If we have more than two elementary links, the entanglement swapping is nested, which requires higher levels of swapping. This leads to the following more general expression for the success probability of entanglement swapping at the i th level [8]:

$$P_i = \frac{p_1 \alpha^2 \eta_{\text{tot}}}{2} \frac{[2^i - (2^i - 1)p_1 \alpha^2 \eta_{\text{tot}}]}{[2^{i-1} - (2^{i-1} - 1)p_1 \alpha^2 \eta_{\text{tot}}]^2}. \quad (12)$$

After the entanglement swapping, a single excitation in noble-gas spins is shared between two remote locations (in Fig. 1(b) it is between A and D). As mentioned before, we need to perform post-selection by reading out the stored photons in each location, which allows us to generate an effective state $1/\sqrt{2}(|k_A k_{D'}\rangle + |k_{A'} k_D\rangle)$. Here the dark counts are negligible because of the short detection time T_d , as mentioned in Sec. III A. Then, the success probability of performing this projection is given by [8]

$$P_{\text{ps}} = \frac{(p_1 \alpha^2 \eta_{\text{tot}})}{2} \frac{1}{[2^i - (2^i - 1)p_1 \alpha^2 \eta_{\text{tot}}]^2}. \quad (13)$$

This post-selection step enables us to eliminate the vacuum components in Eq. (10) as it is impossible to detect a single

photon on each side if both links are vacuum. Hence, the overall fidelity is not affected by the vacuum components in Eq. (10) but as mentioned they have a significant impact on repeater rates.

In the retrieval process, FWM noise can be strongly suppressed by choosing $\phi_s = 0$ (on resonance) and $\phi_a = \pi$ (antiresonance). In the strong-coupling regime, this noise can be quantified by calculating the $g_{\text{re}}^{(2)}$ function of the retrieved signal, which is equal to $2|x|^2 \zeta_1 |\Gamma_s|^2 / |\Gamma_d|^2$ [30] when there is no mode mismatching, and the input signal contains one photon. Here x is the FWM noise suppression factor, which is given by

$$x \approx \frac{1 - \mu_s}{2\mu_s} = \frac{1 - re^{-d(\frac{\gamma_e}{\Delta_s})^2}}{2re^{-d(\frac{\gamma_e}{\Delta_s})^2}}. \quad (14)$$

$\zeta_1 \gg 1$ is the dimensionless coupling strength between both the signal and anti-Stokes field and the alkali gas, which in this case is given by

$$\zeta_1 \approx 2 \left| \frac{\sqrt{C_s \gamma_e W}}{\Gamma_s} \right|^2, \quad (15)$$

where $C_s = d\mu_s/(1 - \mu_s) \approx d/2x$ and $W = \int_0^{T_c} |\Omega(t)|^2 dt$ stands for the integrated Rabi frequency with T_c being the control pulse duration. Then, the readout fidelity is given by

$$F_{\text{re}} = \frac{1}{1 + \text{SNR}^{-1}}, \quad (16)$$

where $\text{SNR}^{-1} = g_{\text{re}}^{(2)}/2$ [30]. Here, we ignore the infidelity that comes from the detector's dark counts as the detection window time is assumed to be around 12.5 ns. Using the parameters discussed in Sec. V, it is possible to have a readout fidelity as high as 98.6%.

IV. REPEATER RATES AND OVERALL FIDELITIES

In our system as the storage and retrieval times are mainly limited by how fast we can transfer the coherence from hot vapor to noble-gas spins via the spin-exchange collisions, and these times are given by $t_{\text{trans}} = \pi/2J$, which is around 1.5 ms based on the parameters in Sec. V. This transfer time is on the same order as the two-way communication time L_0/c for L_0 ranging from 50 to 100 km with $c = 2 \times 10^8$ m/s, which makes the total length of an eight-link repeater ranging from 400 to 800 km. Furthermore, the average charging time t_{ch} in the ensemble also needs to be taken into account as it is comparable to t_{trans} both in a four-link repeater and an eight-link repeater with the final target fidelity $F_{\text{targ}} = 0.9$, as discussed later in this section. Now, taking η_{gen} , P_i , and P_{ps} into the standard entanglement distribution time for the single-photon

protocol [8] plus the extra time spent for retrieving the signal and charging the ensemble, we obtain

$$T_{\text{tot}} = \frac{3^{n+1}}{2} \left(\frac{L_0}{c} + t_{\text{trans}} + t_{\text{ch}} \right) \frac{\prod_{i=1}^n (2^i - (2^i - 1)p_1 \alpha^2 \eta_{\text{tot}})}{\eta_t \eta_c \eta_d p_1^{n+3} \beta^2 \alpha^{2n+4} \eta_{\text{tot}}^{n+2}}, \quad (17)$$

where n indicates the number of nesting levels, and the number of links associated with it is 2^n . Thus, the total length of a repeater is $L = 2^n L_0$. In Fig. 3(a) we plot the four-link case (D), multiplexed four-link case (C), and the eight-link case (E) for the hot hybrid gases-based scheme (referred to as scheme 1) with respect to total distance when $\eta_s = \eta_r = 0.9$ and $F_{\text{targ}} = 0.9$ as discussed below, and we plot the four-link case (G) for scheme 1 with $\eta_s = \eta_r = 0.8$. The choice of the storage (retrieval) efficiency is discussed in detail in Sec. V. Also, we plot the four-link case (B) and the eight-link case (A) for N- V centers and the optomechanics-based scheme (referred to as scheme 2) [19] for comparison. The direct transmission (F) is plotted with a source of 10 GHz. For C, it is multiplexed by a factor of 100, which can be implemented spatially [8,51] or spectrally [12], as discussed in Sec. V. All these repeaters outperform direct transmission at some point but, in general, the rates of scheme 2 are much higher than the rates of scheme 1. The lower rates for scheme 1 are due to the fact that the single-photon protocol is nested as the entanglement swapping and post-selection are probabilistic as opposed to the non-nested scheme used in [19], and the interface between alkali atoms and noble-gas spins is also quite slow, which further degrades the repeater rates. The other factors that limit the repeater rates in this proposal are detection efficiency η_d and frequency conversion efficiency η_c , which could be improved to further enhance the rates. We expect an order of magnitude increase in rates when we increase η_d from 0.6 to 0.9. The slow interface between hot vapor and noble-gas spins also plays a role in reducing the rates, but the room for improving the speed of this interface is limited as it is based on weak spin-exchange interactions [37], which means J cannot be too large. It is worth noting that it is much easier to perform multiplexing in hot hybrid gases-based repeaters than N- V centers and optomechanics-based repeaters because the latter requires much more complex setups than the former [19]. Moreover, there is a trade-off between the target fidelity F_{targ} and repeater rates as F_{targ} determines t_{ch} . However, the improvement in rates is not significant when we set a lower target fidelity.

The infidelities in our repeaters mainly come from multiphoton emissions of the single-photon source and FWM noise in the entanglement swapping and post-selection. The effect of FWM noise in the signal readout is estimated in Sec. III B based on the parameters discussed in Sec. V, which gives us a high readout fidelity of 98.6%. In addition, the decoherence of the noble-gas spins does not

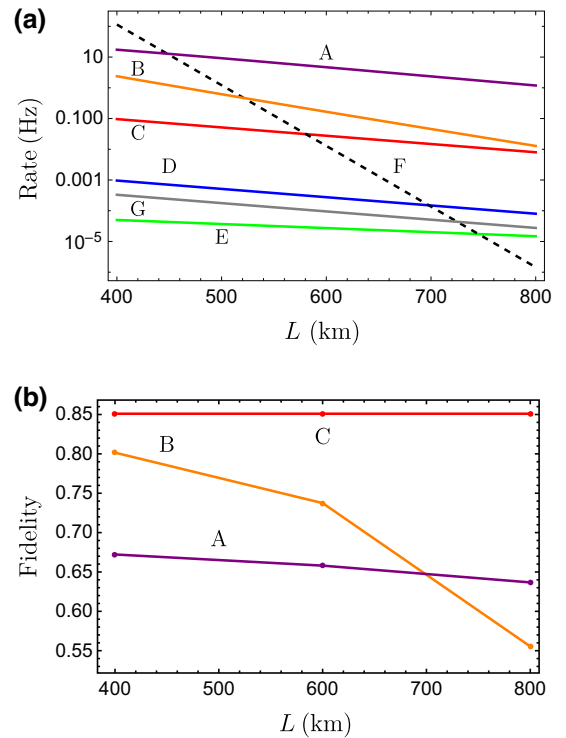


FIG. 3. (a) Repeater rates as a function of total distance L with $F_{\text{targ}} = 0.9$ for a hot hybrid gases-based scheme (referred to as scheme 1), and repeater rates for N- V centers and an optomechanics-based scheme (referred to as scheme 2) [19] with corresponding fidelities shown in (b). Here, we plot the four-link case (B) and eight-link case (A) for scheme 2, and we also plot the four-link case (D), multiplexed four-link case (C), and eight-link case (E) for scheme 1 with the efficiency $\eta_s = \eta_r = 0.9$, and the four-link case (G) for scheme 1 with efficiency $\eta_s = \eta_r = 0.8$. The choice of the storage (retrieval) efficiency is justified in Sec. V. The direct transmission (F) is plotted with a single-photon source of 10 GHz. For C, it is multiplexed by a factor of 100. In general, the rates of scheme 2 are much higher than the rates of scheme 1. All these repeaters outperform direct transmission. We assume that $\eta_c = 0.8$, $\eta_d = 0.6$, $\alpha^2 = 0.84$, $\beta^2 = 0.16$, $t_{\text{trans}} = 1.5$ ms for all cases in scheme 1. We also use $t_{\text{ch}} = 0.048$ ms for D and G, and 1.03 ms for E. The emission probability for the single-photon source p_1 is assumed to be 0.9 for all repeaters in both schemes. (b) Repeater fidelities as a function of total distance L for schemes 1 and 2. A and B are eight-link and four-link cases in scheme 2 [19]. Here C stands for a 100-multiplexed four-link repeater in scheme 1 with $F_{\text{targ}} = 90\%$ and $F_{\text{re}} = 98.6\%$. As a multiplexed eight-link repeater in scheme 1 has fidelities very close to C, it is not shown here. In general, scheme 1 yields much higher fidelities than scheme 2, and they are independent of the total distance.

affect the final fidelities as we perform post-selection in the end to filter out the vacuum components. Now, the overall fidelity is given by

$$F_{\text{tot}} = F_{\text{targ}} \times (F_{\text{re}})^{n+2}, \quad (18)$$

where $n + 2$ is the number of performing readouts and F_{targ} is a target fidelity of repeaters, which we choose to be 90% for all repeaters in scheme 1 with different nesting levels. This fidelity is determined by errors due to multiphoton emission in the ensemble-based single-photon source [8]. The probability of having a two-photon contribution is given by $p_2 = 2p(1 - \eta_{\text{st}})p_1$, where p is the probability of emitting the Stokes photon when charging the ensemble and η_{st} is the efficiency of detecting a Stokes photon, assumed to be 0.75 using a silicon single-photon detector [49,50]. In order to make p_2 small enough to have $F_{\text{targ}} = 0.9$, we need to make p sufficiently small. It can be shown that when we have a four-link repeater, the maximum value that p_2 can take is 0.00093 [8], which leads to $p = 0.0021$. This emission probability results in a charging time given by $t_{\text{ch}} = 1/(Rp) = 0.048$ ms with the repetition rate $R = 10$ MHz. If we have an eight-link repeater with $F_{\text{targ}} = 0.9$, we obtain $p = 9.73 \times 10^{-5}$, which leads to $t_{\text{ch}} = 1.03$ ms. Assuming the readout fidelity for both swapping and post-selection is 98.6%, the overall fidelities of a four-link and eight-link repeater in scheme 1 are estimated to be 85.1% and 83.87%. In Fig. 3(b) we plot the overall fidelities as a function of the total distance L for scheme 1 and scheme 2. A and B are eight-link and four-link repeaters in scheme 2 that decrease as the total distance increases due to thermal noise present in the system, which are treated as dark counts [19]. C is the multiplexed four-link repeater in scheme 1, which is independent of the total distance. In general, scheme 1 yields fidelities that are significantly higher than the fidelities in scheme 2, which is mainly due to the fact that the accumulated infidelities induced by vacuum components are eliminated in the end by post-selection. Overall, these two schemes have their own advantages and disadvantages. Scheme 1 is much slower than scheme 2 but has much higher fidelities, and scheme 1 requires much less complex setups than scheme 2 that also facilitates multiplexing. Moreover, it is possible to boost the fidelities using entanglement purification [52], but this comes at the cost of further reducing the rates. A quantitative discussion of repeaters including purification goes beyond the scope of the present work.

V. IMPLEMENTATION

Here, we consider ^{39}K atoms as the hot vapor and ^3He atoms as the noble-gas spins in our system, where the optical depth d of the hot vapor is assumed to be 100, which can be achieved in the high-density hot vapors. The linewidth of the excited state $2\gamma_e$ is taken to be 27 GHz for the broadened D_1 line due to collisions with the buffer gas, which is much smaller than the assumed detuning $\Delta_s = 2700$ GHz so it makes the system in the far-off-resonant regime [30]. Moreover, such a large detuning Δ_s also makes the Doppler broadening negligible, around 1

GHz at 230°C. But this often comes at the cost of reducing the efficiency due to large detuning so we also need to make sure the system is still in the strong-coupling regime in the far-off-resonant regime, which then requires a strong control pulse as discussed below in this section. In fact, it has been shown that at high enough optical depth (or high enough cooperativity), the effect of Doppler broadening or any inhomogeneous broadening is negligible [53]. So far, the experimentally achieved value of J is around 78 Hz [39], but if we further increase the pressure to increase the gas densities, it is possible to have $J = 1000$ Hz [37]. In this condition, for γ_s and γ_k , they are estimated to be 17.5 Hz and 2.8×10^{-6} Hz, respectively, dominated by intragas and intergas collisional spin-rotation couplings [37–39]. However, one also needs to take the diffusion-induced effect into account. For the single uniform mode of the alkali atoms, the diffusion-induced decay rate is given by $D_a\pi^2/R^2$, where D_a is the diffusion coefficient of the alkali atoms and R is the radius of the spherical cell. For a cell with $R \sim 0.15$ cm, in a high buffer-gas pressure configuration ($D_a = 0.054$ cm²/s) the diffusion-induced decay rate is estimated to be around 28 Hz. Thus, the actual decay rate of ^{39}K atoms γ_s is the sum of the original rate and the diffusion-induced rate, which becomes 45.5 Hz. For the single uniform mode of the noble-gas atoms, the spatial diffusion does not affect its own decay rate, thus leaving γ_k unchanged. To verify that we are in the light-dominated regime, the power broadening due to the control beam is $\text{Re}(|\Omega|^2(1/\Gamma_s + 1/\Gamma_a^*))$, which is around 3700 Hz; thus, much larger than the diffusion-induced decay rate of 28 Hz. Overall, this yields a storage efficiency of around 90%. In real experiments this efficiency could be lower due to possible mode mismatch in the cavity, so we also use a lower value of 80% in calculating repeater rates and fidelities in Fig. 3.

Moreover, $\Delta_a = \Delta_s + \delta_s$, where δ_s is the splitting between the states $|g\rangle$ and $|s\rangle$, which is around 0.46 GHz in ^{39}K vapor. The dimensionless coupling strength ζ_1 is taken to be 10 to ensure we are in the strong-coupling regime, which could be achieved by using a square pulse as the control field with the Rabi frequency $\Omega \sim 2\pi \times 1$ GHz and the duration $T_c \sim 50$ ns. The power of the control laser can be related to the Rabi frequency as $P = (\hbar\Omega/d_i)^2 c\epsilon_0\pi R_w^2/2$, where d_i is the dipole moment of the D_1 line, ϵ_0 is the vacuum permittivity, and R_w is the waist width of the control beam. Then, given the waist is on the same order as the radius of the cell, approximately 0.15 cm, the required power of the control laser is estimated to be around 2 W, and the energy is 100 nJ. In general, the larger the signal detuning Δ_s is, the more difficult it is to achieve the strong-coupling regime as we need a stronger and longer control pulse, which can be seen from Eq. (15). In the strong-coupling regime, the noise suppression factor x is given in Eq. (14), and when the storage and retrieval efficiencies are optimized, the reflectivity r is given by $r =$

$(1 - \sqrt{1 - \alpha_s^2})/\alpha_s$ with $\alpha_s \approx \exp\{-d(\gamma_e/\Delta_s)^2\}$, which is estimated to be 93.2%. Thus, we obtain the signal readout fidelity $F_{\text{re}} \sim 98.6\%$. The cavity linewidth κ_c is linked to r and the hyperfine splitting δ_s as $\kappa_c = 8\delta_s(1 - r)/r$, which is estimated to be 0.27 GHz. Moreover, in the bad-cavity regime the bandwidth δ_B of this hybrid quantum memory is upper bounded by the cavity linewidth as $0.3\kappa_c$ [30], which gives $\delta_B \sim 80$ MHz. The size of the ring cavity is given by the length of the roundtrip $L = \pi c/(2\delta_s) = 160$ mm. As for the time-bandwidth product, this hybrid quantum memory yields an unprecedented value of 2.8×10^{13} that is mainly attributed to the hours-long storage time in the noble gas and the large bandwidth of the hot vapor. The multiplexing can be implemented either spatially or spectrally. For spatial multiplexing, we envision having many hybrid memories in each node [51]. Spectral multiplexing also requires many hybrid memories in one node but the emitted photons need to be converted to different frequencies fed into a common channel [12,54]. This can be accomplished using frequency translation that can be noise-free using waveguide electro-optic modulators [55]. The feeding to a common channel can be achieved by a tunable ring resonator filter that enables megahertz-level resonance linewidths [56].

VI. CONCLUSIONS AND OUTLOOK

We present a quantum network architecture based on hot hybrid alkali-noble gases that can operate without cryogenics. We show that under realistic conditions, high-fidelity entanglement can be distributed over long distances thanks to the ultralong coherence time of noble-gas spins. We show that the rates of our proposed quantum repeaters can outperform direct transmission, and with realistic multiplexing, the rates can be greatly enhanced, close to the corresponding rates of N- V centers and optomechanics-based repeaters. Furthermore, compared with the complex setup in room-temperature repeaters based on N- V centers and optomechanics, this hybrid gas system only requires a moderate-finesse ring cavity, an external magnetic field, and optical pumping equipment. This significantly reduces the complexity of the system while offering a great potential to be scalable. We hope that this work could further stimulate the development of high-efficiency silicon single-photon detectors and even room-temperature detectors that offer both high detection efficiencies and low dark count rates for telecom photons.

Here we focus on hot atomic gas-based quantum repeaters on the ground, but this compact hybrid quantum system also offers a good potential for being used as memory in space [25], which could unlock the possibility of establishing a truly global quantum network [57–59] that goes beyond the limit of terrestrial quantum repeaters, and

such a global quantum network could enable ultralong-distance quantum teleportation, quantum entanglement, and applications in fundamental physics tests [25].

ACKNOWLEDGMENTS

We thank A. Sørensen and J. Nunn for helpful discussions. This work is supported by the Natural Sciences and Engineering Research Council of Canada (NSERC) through its Discovery Grant (DG), CREATE, and Strategic Project Grant (SPG) programs, and by the National Research Council (NRC) of Canada through its High-Throughput Secure Networks (HTSN) challenge program, and by Alberta Innovates Technology Futures (AITF) Graduate Student Scholarship (GSS) program.

J.-W.J., F.K.A., and C.S. acknowledge that the University of Calgary is located on the traditional territories of the people of the Treaty 7 region in Southern Alberta, which includes the Blackfoot Confederacy (comprising the Siksika, Piikani, and Kainai First Nations), as well as the Tsuut'ina First Nation, and the Stoney Nakoda (including the Chiniki, Bearspaw, and Wesley First Nations). The City of Calgary is also home to the Métis Nation of Alberta (Region 3). K.H. acknowledges that the NRC headquarters is located on the traditional unceded territory of the Anishinaabe and Mohawk people.

-
- [1] N. Gisin, G. Ribordy, W. Tittel, and H. Zbinden, Quantum cryptography, *Rev. Mod. Phys.* **74**, 145 (2002).
 - [2] S. Barz, E. Kashefi, A. Broadbent, J. F. Fitzsimons, A. Zeilinger, and P. Walther, Demonstration of blind quantum computing, *Science* **335**, 303 (2012).
 - [3] M. Jakobi, C. Simon, N. Gisin, J.-D. Bancal, C. Branciard, N. Walenta, and H. Zbinden, Practical private database queries based on a quantum-key-distribution protocol, *Phys. Rev. A* **83**, 022301 (2011).
 - [4] H. J. Kimble, The quantum internet, *Nature* **453**, 1023 (2008).
 - [5] C. Simon, Towards a global quantum network, *Nat. Photonics* **11**, 678 (2017).
 - [6] S. Wehner, D. Elkouss, and R. Hanson, Quantum internet: A vision for the road ahead, *Science* **362**, 6412 (2018).
 - [7] W. K. Wootters and W. H. Zurek, A single quantum cannot be cloned, *Nature* **299**, 802 (1982).
 - [8] N. Sangouard, C. Simon, H. de Riedmatten, and N. Gisin, Quantum repeaters based on atomic ensembles and linear optics, *Rev. Mod. Phys.* **83**, 33 (2011).
 - [9] S. Muralidharan, L. Li, J. Kim, N. Lütkenhaus, M. D. Lukin, and L. Jiang, Optimal architectures for long distance quantum communication, *Sci. Rep.* **6**, 20463 (2016).
 - [10] L.-M. Duan, M. D. Lukin, J. I. Cirac, and P. Zoller, Long-distance quantum communication with atomic ensembles and linear optics, *Nature* **414**, 413 (2001).
 - [11] S. Kumar, N. Lauk, and C. Simon, Towards long-distance quantum networks with superconducting processors and optical links, *Quantum Sci. Technol.* **4**, 045003 (2019).

- [12] F. Kimiaee Asadi, N. Lauk, S. Wein, N. Sinclair, C. O'Brien, and C. Simon, Quantum repeaters with individual rare-earth ions at telecommunication wavelengths, *Quantum* **2**, 93 (2018).
- [13] A. Tchebotareva, S. L. N. Hermans, P. C. Humphreys, D. Voigt, P. J. Harmsma, L. K. Cheng, A. L. Verlaan, N. Dijkhuizen, W. de Jong, A. Dréau, and R. Hanson, Entanglement between a Diamond Spin Qubit and a Photonic Time-Bin Qubit at Telecom Wavelength, *Phys. Rev. Lett.* **123**, 063601 (2019).
- [14] P. C. Humphreys, N. Kalb, J. P. J. Morits, R. N. Schouten, R. F. L. Vermeulen, D. J. Twitchen, M. Markham, and R. Hanson, Deterministic delivery of remote entanglement on a quantum network, *Nature* **558**, 268 (2018).
- [15] A. Delteil, Z. Sun, W.-b. Gao, E. Togan, S. Faelt, and A. Imamoglu, Generation of heralded entanglement between distant hole spins, *Nat. Phys.* **12**, 218 (2016).
- [16] R. Stockill, M. J. Stanley, L. Huthmacher, E. Clarke, M. Hugues, A. J. Miller, C. Matthiesen, C. Le Gall, and M. Atatüre, Phase-Tuned Entangled State Generation between Distant Spin Qubits, *Phys. Rev. Lett.* **119**, 010503 (2017).
- [17] F. K. Asadi, S. C. Wein, and C. Simon, Protocols for long-distance quantum communication with single ^{167}Er ions, *Quantum Science and Technology* **5**, 45015 (2020).
- [18] R. Ghobadi, S. Wein, H. Kaviani, P. Barclay, and C. Simon, Progress toward cryogen-free spin-photon interfaces based on nitrogen-vacancy centers and optomechanics, *Phys. Rev. A* **99**, 053825 (2019).
- [19] J.-W. Ji, Y.-F. Wu, S. C. Wein, F. K. Asadi, R. Ghobadi, and C. Simon, Proposal for room-temperature quantum repeaters with nitrogen-vacancy centers and optomechanics, *Quantum* **6**, 669 (2022).
- [20] J. Borregaard, M. Zugenmaier, J. M. Petersen, H. Shen, G. Vasilakis, K. Jensen, E. S. Polzik, and A. S. Sørensen, Scalable photonic network architecture based on motional averaging in room temperature gas, *Nat. Commun.* **7**, 11356 (2016).
- [21] H. Li, J.-P. Dou, X.-L. Pang, T.-H. Yang, C.-N. Zhang, Y. Chen, J.-M. Li, I. A. Walmsley, and X.-M. Jin, Heralding quantum entanglement between two room-temperature atomic ensembles, *Optica* **8**, 925 (2021).
- [22] M. Zugenmaier, K. B. Dideriksen, A. S. Sørensen, B. Albrecht, and E. S. Polzik, Long-lived non-classical correlations towards quantum communication at room temperature, *Comm. Phys.* **1**, 76 (2018).
- [23] J. P. Dou, A. L. Yang, M. Y. Du, D. Lao, J. Gao, L. F. Qiao, H. Li, X. L. Pang, Z. Feng, H. Tang, and X. M. Jin, A broadband DLCZ quantum memory in room-temperature atoms, *Comm. Phys.* **1**, 55 (2018).
- [24] K. B. Dideriksen, R. Schmieg, M. Zugenmaier, and E. S. Polzik, Room-temperature single-photon source with near-millisecond built-in memory, *Nat. Commun.* **12**, 3699 (2021).
- [25] M. Gündoğan *et al.*, Topical white paper: A case for quantum memories in space (2021), arXiv preprint [arXiv:2111.09595](https://arxiv.org/abs/2111.09595).
- [26] N. B. Phillips, A. V. Gorshkov, and I. Novikova, Optimal light storage in atomic vapor, *Phys. Rev. A* **78**, 023801 (2008).
- [27] N. Lauk, C. O'Brien, and M. Fleischhauer, Fidelity of photon propagation in electromagnetically induced transparency in the presence of four-wave mixing, *Phys. Rev. A - At., Mol., Opt. Phys.* **88**, 13823 (2013).
- [28] K. Zhang, J. Guo, L. Q. Chen, C. Yuan, Z. Y. Ou, and W. Zhang, Suppression of the four-wave-mixing background noise in a quantum memory retrieval process by channel blocking, *Phys. Rev. A* **90**, 033823 (2014).
- [29] G. Romanov, C. O'Brien, and I. Novikova, Suppression of the four-wave mixing amplification via Raman absorption, *J. Mod. Opt.* **63**, 2048 (2016).
- [30] J. Nunn, J. H. Munns, S. Thomas, K. T. Kaczmarek, C. Qiu, A. Feizpour, E. Poem, B. Brecht, D. J. Saunders, P. M. Ledingham, D. V. Reddy, M. G. Raymer, and I. A. Walmsley, Theory of noise suppression in Λ -type quantum memories by means of a cavity, *Phys. Rev. A* **96**, 12338 (2017).
- [31] S. E. Thomas, T. M. Hird, J. H. D. Munns, B. Brecht, D. J. Saunders, J. Nunn, I. A. Walmsley, and P. M. Ledingham, Raman quantum memory with built-in suppression of four-wave-mixing noise, *Phys. Rev. A* **100**, 33801 (2019).
- [32] D. J. Saunders, J. H. Munns, T. F. Champion, C. Qiu, K. T. Kaczmarek, E. Poem, P. M. Ledingham, I. A. Walmsley, and J. Nunn, Cavity-Enhanced Room-Temperature Broadband Raman Memory, *Phys. Rev. Lett.* **116**, 090501 (2016).
- [33] K. Hammerer, A. S. Sørensen, and E. S. Polzik, Quantum interface between light and atomic ensembles, *Rev. Mod. Phys.* **82**, 1041 (2010).
- [34] O. Katz and O. Firstenberg, Light storage for one second in room-temperature alkali vapor, *Nat. Commun.* **9**, 2074 (2018).
- [35] M. V. Balabas, T. Karaulanov, M. P. Ledbetter, and D. Budker, Polarized Alkali-Metal Vapor with Minute-Long Transverse Spin-Relaxation Time, *Phys. Rev. Lett.* **105**, 070801 (2010).
- [36] T. R. Gentile, P. J. Nacher, B. Saam, and T. G. Walker, Optically polarized ^3He , *Rev. Mod. Phys.* **89**, 045004 (2017).
- [37] O. Katz, R. Shaham, and O. Firstenberg, Quantum Interface for Noble-Gas Spins Based on Spin-Exchange Collisions, *PRX Quantum* **3**, 010305 (2022).
- [38] O. Katz, R. Shaham, and O. Firstenberg, Coupling light to a nuclear spin gas with a two-photon linewidth of five millihertz, *Sci. Adv.* **7**, 14 (2021).
- [39] R. Shaham, O. Katz, and O. Firstenberg, Strong coupling of alkali-metal spins to noble-gas spins with an hour-long coherence time, *Nat. Phys.* **18**, 506 (2022).
- [40] O. Katz, R. Shaham, E. Reches, A. V. Gorshkov, and O. Firstenberg, Optical quantum memory for noble-gas spins based on spin-exchange collisions, *Phys. Rev. A* **105**, 042606 (2022).
- [41] N. Sangouard, C. Simon, J. c. v. Minář, H. Zbinden, H. de Riedmatten, and N. Gisin, Long-distance entanglement distribution with single-photon sources, *Phys. Rev. A* **76**, 050301 (2007).
- [42] Y. Kubo, F. R. Ong, P. Bertet, D. Vion, V. Jacques, D. Zheng, A. Dréau, J.-F. Roch, A. Auffèves, F. Jelezko, J. Wrachtrup, M. F. Barthe, P. Bergonzo, and D. Esteve, Strong Coupling of a Spin Ensemble to a Superconducting Resonator, *Phys. Rev. Lett.* **105**, 140502 (2010).

- [43] A. V. Gorshkov, A. André, M. D. Lukin, and A. S. Sørensen, Photon storage in Λ -type optically dense atomic media. I. Cavity model, *Phys. Rev. A* **76**, 033804 (2007).
- [44] P. S. Michelberger, T. F. M. Champion, M. R. Sprague, K. T. Kaczmarek, M. Barbieri, X. M. Jin, D. G. England, W. S. Kolthammer, D. J. Saunders, J. Nunn, and I. A. Walmsley, Interfacing GHz-bandwidth heralded single photons with a warm vapour Raman memory, *New J. Phys.* **17**, 43006 (2015).
- [45] F. Ripka, H. Kübler, R. Löw, and T. Pfau, A room-temperature single-photon source based on strongly interacting Rydberg atoms, *Science* **362**, 446 (2018).
- [46] O. Davidson, R. Finkelstein, E. Poem, and O. Firstenberg, Bright multiplexed source of indistinguishable single photons with tunable GHz-bandwidth at room temperature, *New J. Phys.* **23**, 73050 (2021).
- [47] M.-Y. Zheng, Q. Yao, B. Wang, X.-P. Xie, Q. Zhang, and J.-W. Pan, Integrated Multichannel Lithium Niobate Waveguides for Quantum Frequency Conversion, *Phys. Rev. Appl.* **14**, 034035 (2020).
- [48] J. c. v. Minář, H. de Riedmatten, C. Simon, H. Zbinden, and N. Gisin, Phase-noise measurements in long-fiber interferometers for quantum-repeater applications, *Phys. Rev. A* **77**, 052325 (2008).
- [49] Y.-Q. Fang, K. Luo, X.-G. Gao, G.-Q. Huo, A. Zhong, P.-F. Liao, P. Pu, X.-H. Bao, Y.-A. Chen, J. Zhang, and J.-W. Pan, High detection efficiency silicon single-photon detector with a monolithic integrated circuit of active quenching and active reset, *Rev. Sci. Instrum.* **91**, 123106 (2020).
- [50] M. A. Wayne, J. C. Bienfang, and A. L. Migdall, Low-noise photon counting above 100×106 counts per second with a high-efficiency reach-through single-photon avalanche diode system, *Appl. Phys. Lett.* **118**, 134002 (2021).
- [51] O. A. Collins, S. D. Jenkins, A. Kuzmich, and T. A. B. Kennedy, Multiplexed Memory-Insensitive Quantum Repeaters, *Phys. Rev. Lett.* **98**, 060502 (2007).
- [52] D. Salart, O. Landry, N. Sangouard, N. Gisin, H. Herrmann, B. Sanguinetti, C. Simon, W. Sohler, R. T. Thew, A. Thomas, and H. Zbinden, Purification of Single-Photon Entanglement, *Phys. Rev. Lett.* **104**, 180504 (2010).
- [53] A. V. Gorshkov, A. André, M. D. Lukin, and A. S. Sørensen, Photon storage in Λ -type optically dense atomic media. III. Effects of inhomogeneous broadening, *Phys. Rev. A* **76**, 033806 (2007).
- [54] Q. Glorieux, J. B. Clark, A. M. Marino, Z. Zhou, and P. D. Lett, Temporally multiplexed storage of images in a gradient echo memory, *Opt. Express* **20**, 12350 (2012).
- [55] M. Grimau Puigibert, G. H. Aguilar, Q. Zhou, F. Marsili, M. D. Shaw, V. B. Verma, S. W. Nam, D. Oblak, and W. Tittel, Heralded Single Photons Based on Spectral Multiplexing and Feed-Forward Control, *Phys. Rev. Lett.* **119**, 083601 (2017).
- [56] K. Y. Yang, D. Y. Oh, S. H. Lee, Q.-F. Yang, X. Yi, B. Shen, H. Wang, and K. Vahala, Bridging ultrahigh-Q devices and photonic circuits, *Nat. Photonics* **12**, 297 (2018).
- [57] M. Gündoğan, J. S. Sidhu, V. Henderson, L. Mazzarella, J. Wolters, D. K. L. Oi, and M. Krutzik, Proposal for spaceborne quantum memories for global quantum networking, *Npj Quantum Inf.* **7**, 128 (2021).
- [58] C. Liorni, H. Kampermann, and D. Bruß, Quantum repeaters in space, *New J. Phys.* **23**, 53021 (2021).
- [59] K. Boone, J.-P. Bourgoin, E. Meyer-Scott, K. Heshami, T. Jennewein, and C. Simon, Entanglement over global distances via quantum repeaters with satellite links, *Phys. Rev. A* **91**, 052325 (2015).